ACS Photonics

pubs.acs.org/journal/apchd5

Article

Hybrid Interfacial Engineering: An Enabling Strategy for Highly Sensitive and Stable Perovskite Quantum Dots/Organic Heterojunction Phototransistors

Yuanhong Gao, Shuai Sun, Dan Qiu, Yu-Ming Wei, Mengpei Zhang, Jin Liu, Paul K. Chu, Wen-Long You, and Jia Li*

Cite This: *ACS Photonics* 2023, 10, 764−771

Read Online

ACCESS | Metrics & More | Article Recommendations | Supporting Information

ABSTRACT: All-inorganic lead halide perovskite quantum dots (PQD) have attracted tremendous research interest in the field of phototransistors due to their excellent optoelectronic properties. However, the inefficient charge transport/extraction and high trap-state density of the assembled PQD films seriously limit the photoresponsivity of PQD-based phototransistors. Herein, we demonstrate that these limits can be overcome by adopting a novel device architecture composed of a polar-polymer capping layer on a PQD/organic semiconductor (OSC) heterojunction. The polar polymer film plays the role of both electron trapping and encapsulation, whereas OSC provides the fast transport tracks for charges and PQD serves as the photoactive materials. Owing to the balanced dynamic processes of photogenerated charges, highly sensitive photodetection is achieved, as demonstrated by the peak photosensitivity of 1.5×10^4, a photoresponsivity of 2.1×10^4 A/W, a detectivity of 1×10^{15} Jones, and a high gain of 6.4×10^4 under weak incident light of 3 μW/cm^2. Additionally, the phototransistors exhibit superior stability and reproducibility with negligible changes in the output current both in darkness and under illumination after storing for 4 months. The results demonstrate the promising potentials of the polar polymer/PQD/OSC heterojunction for high-performance photodetectors, and the mechanism and strategy described here can be applied to other kinds of quantum dots-based optoelectronic devices.

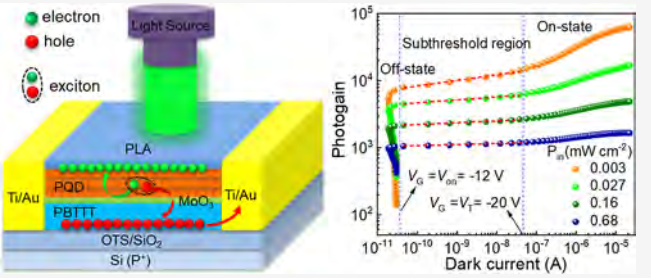

KEYWORDS: *phototransistors, inorganic lead halide perovskite, quantum dots, organic semiconductors, polar polymer*

1. INTRODUCTION

Phototransistors, as one type of photodetectors that directly convert optical signals into electrical signals, have been widely applied to image sensing,[1−4] environmental/health monitoring,[5−7] chemical/biomedical sensing,[8,9] X-ray detection,[10,11] and quantum communication.[12,13] Among the various semiconductors used as photoactive materials in the phototransistors, all-inorganic perovskites ($CsPbX_3$, X = Cl, Br, and I) quantum dots (PQD) stand out due to the superior optoelectronic properties,[14] such as efficient photon absorption, long carrier diffusion length, intrinsically high mobility, and unprecedented photon-to-electron conversion efficiency, consequently offering a great opportunity to develop high-performance phototransistors.[11,15−21] However, despite recent advances, the performance of most reported PQD-based phototransistors needs improvement. This is mainly caused by the low carrier extraction/transport efficiency and large trap-state density of solution-assembled PQD films. Moreover, the low stability of PQD hinders its practical applicability in devices.[22]

The key to overcoming the aforementioned challenges is to increase the carrier diffusion length and reduce the carrier recombination rate. In this context, a layered heterojunction has been recognized as an effective approach optimizing the carrier dynamic process, facilitating the extraction/transportation of photogenerated carriers, and improving the photoresponsivity of PQD-based phototransistors. Kwak, et al.[23] have exploited graphene as the fast carrier tracks and incorporated $CsPbBr_{3-x}I_x$ quantum dots/graphene layered heterojunction into phototransistors, leading to ultrahigh responsivity (10^8 A/W) and detectivity (10^{16} Jones), but the noise current cannot be turned off in the dark, thus resulting in a low photo-current to dark-current ratio (I_{light}/I_{dark}). Chen et al.[15] have proposed the $CsPbBr_3$ QDs/DNTT-layered heterojunction to compensate for the low conductivity of the PQD film. The phototransistor exhibits significantly improved photoresponsivity and I_{light}/I_{dark}. However, the PQD sand-

Received: December 17, 2022
Published: February 22, 2023

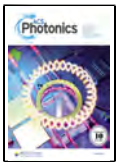

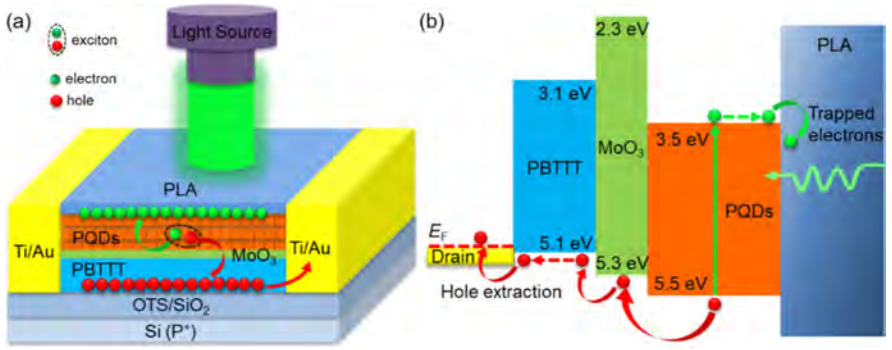

Figure 1. Schematic showing the structure of the HJPT and corresponding photodetection mechanism. (a) Illustration of Frenkel excitons generation under light illumination, hole transport in the channel, and the electron trapping process at the PQDs/PLA interface; (b) energy level diagram of the HJPT device under illumination.

wiched between the organic semiconductor and dielectric layer deteriorates carrier transportation because the conduction channel is typically located at the first few molecular layers (~10 nm) near the dielectric layer. Although these pioneering works have demonstrated the important role of LHJ in enhancing the photodetection characteristics, it is still necessary to further optimize the dynamic process of charge carriers in order to improve the photodetection properties.

The charge-trapping effect (CTE) based on donor/acceptor (D/A) heterojunctions offers an effective strategy to tailor the charge transport/recombination processes to enhance the photodetection performance.[24−26] One possible way to achieve CTE is to integrate polar polymers, such as poly(methyl methacrylate) or polylactide (PLA) into OSC, so that CTE occurs at the polar polymer/OSC interface due to the existence of electron-capturing moieties in the polar polymers, leading to significantly suppressed electron−hole recombination. Herein, a polar polymer-capped PQD/OSC heterojunction is designed and demonstrated for phototransistors. By taking advantages of CTE and building a fast transport pathway for photogenerated charges, balanced charge separation and transport are achieved, resulting in ultrasensitive photodetection. In addition, the device stability and reproducibility are greatly improved on account of the kinetic barriers formed by the PLA-protective layer.

The heterojunction phototransistor (HJPT) is constructed by using a P-type OSC, poly[2,5-bis(3-tetradecylthiophen-2-yl)thieno[3,2-*b*]thiophene] (PBTTT or PBT), as the fast carrier transport pathway, $CsPbBrI_2$ perovskite quantum dots (PQD) as the efficient photosensitive layer, MoO_3 as the hole injection layer, and PLA as the electron trapping layer. PLA not only provides the electron-capturing moieties to trap photo-generated electrons but also serves as a kinetic barrier to prevent the devices from moisture/oxygen degradation and improve the device stability and reproducibility. Upon light illumination, the photo-generated electrons can be trapped by the polar polymer, and at the same time, holes can be extracted quickly by OSC, thus resulting in both high gain and fast carrier transport. As a result, superior photodetection properties are obtained from the PLA/PQD/MoO_3/PBTTT HJPT by combining efficient light absorption, high conductivity, as well as the high-gain effect. The fabricated HJPT delivers outstanding photodetection performance, such as a photosensitivity of 1.5×10^4, a photoresponsivity of 2.1×10^4 A/W, a photodetectivity of 1×10^{15} Jones, and a high gain of 6.4×10^4 under a weak incident light of 3 μW/cm^2. Furthermore, the HJPT exhibits excellent stability and reproducibility, with negligible changes in both the output current in the dark and under illumination after storing under ambient conditions for 4 months. These results demonstrate that the device architecture based on the polar-polymer/PQD/OSC heterojunction is promising for high-performance photodetectors. Moreover, the mechanism and strategy described here provide a general platform to develop other QD-based high-performance optoelectronic devices.

2. RESULTS AND DISCUSSION

To implement our device concept, the HJPT is fabricated with a bottom-gate/bottom-contact transistor geometry on the SiO_2/p + -Si substrate (Figure 1a). Before fabrication, the substrate is cleaned by a standard process and precoated with an octyltrichlorosilane (OTS) self-assembled monolayer to facilitate the formation of the high-quality organic conduction channel. The Ti/Au (5 nm/50 nm) source/drain electrodes are evaporated thermally on the pretreated substrate through a shadow mask. Afterwards, PBTTT, MoO_3, PQD, and PLA are deposited sequentially on the prepatterned substrate with thicknesses of 20, 5, 100, and 300 nm, respectively. To demonstrate the improved photodetection characteristics after adding the PLA layer, a reference phototransistor is also prepared without the PLA layer. An inorganic MoO_3 interlayer is introduced on the PBTTT layer to prevent the PBTTT from degradation by the solvent and decrease the defect states during the subsequent solution-based coating process. Besides, it also acts as charge transport materials to spatially separated photo-generated holes/electrons to suppress electron−hole recombination. The important role of the MoO_3 interlayer in the photodetection performance has been verified previously.[27] The biopolymer PLA is cost-effective and has good biocompatibility. More importantly, the abundant carbonyl groups in PLA provide electron-capturing moieties that can interact with PQD to induce CTE at the interface[24,28] to reduce the dark current for efficient exciton dissociation. Moreover, PLA serves as an encapsulation layer to prevent the underlying PQD/PBTTT heterojunction from degrading by oxygen/moisture transmission.[29,30] Consequently, the device stability is improved significantly.

Atomic force microscopy (AFM) is employed to examine the surface morphological changes after film deposition for each layer, as shown in Figure 2a. No obvious changes in the surface morphology and root mean square (RMS) roughness are observed after the deposition of the ultrathin MoO_3

https://doi.org/10.1021/acsphotonics.2c01983
ACS Photonics 2023, 10, 764−771

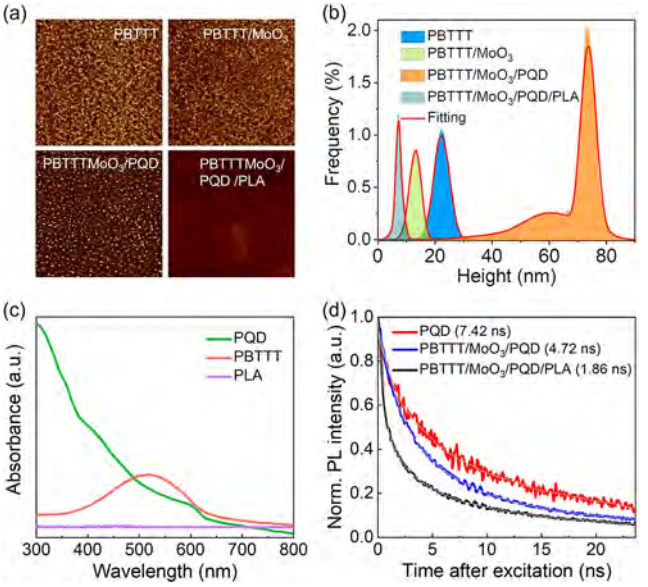

Figure 2. (a) AFM images (10 μm × 10 μm) of PBTTT (top-left), PBTTT/MoO_3 (top-right), PBTTT/MoO_3/PQD (bottom-left), and PBTTT/MoO_3/PQD/PLA (bottom-right); (b) corresponding height distributions derived from the AFM results shown in (a); (c) UV−vis absorbance spectra of PQDs, PBTTT, and PLA; (d) steady-state PL spectra of the PBTTT, PQD, and PLA thin films.

interlayer, revealing that the original characteristics of PBTTT are preserved. After spin-coating PQD, clear grain-like surface features appear, and the RMS roughness increases from 1.6 to 7.52 nm. Finally, deposition of the PLA layer reduces the RMS roughness to 1.3 nm. The corresponding height distributions determined from the AFM data are presented in Figure 2b, and an asymmetric height distribution is observed from the PQD surface. This can be attributed to the coexistence of PQD-aggregation regions and thin PQD areas, which is consistent with the high RMS roughness of the PQD films. The Gaussian-like distribution can be observed in all other film configurations, indicative of good uniformity and smoothness. Figure 2c presents the ultraviolet visible (UV−vis) absorption spectra of the PQD, PBTTT, and PLA films deposited on quartz. Both absorption edges of PQD and PBTTT appear slightly below 620 nm, while no absorbance is observed from the PLA film in the wavelength range of 300−800 nm, indicating that the PLA layer is optically transparent to UV and visible light. Figure 2d displays the transient photoluminescence (PL) decay spectra of the PQD, PBTTT/MoO_3/PQD, and PBTTT/MoO_3/PQD/PLA films. Clearly, the PL signal from the heterojunction film with PLA decays faster than that of the films without PLA, implying efficient charge transfer or trapping at the PQD/PLA heterointerface. The abundant polar groups in PLA provide electron-capturing moieties that can interact with PQD to induce CTE at the interface to improve the electron−hole pair separation efficiency, giving rise to a shorter PL lifetime.

Fast carrier transport is vital to sensitive phototransistors, as the high carrier mobility in the conduction channel enhances carrier collection and transport, leading to high photosensitivity and responsivity. Before determining the photodetection properties of the HJPT, the basic transistor characteristics are assessed in the dark. The transfer characteristics of the field-effect transistors consisting of PQD, PBT, PBT/PQD, and PBT/MoO_3/PQD are presented in Figure 3a,b. With regard to the PQD transistors, V_D is fixed at −5 V, and the linear mobility (μ_{lin}) is determined to be ~6.5 × 10^{-5} cm^2 V^{-1} s^{-1} according to the linear transfer curves. The low carrier mobility arises from the high density of defect states in the assembled PQD films and significantly limits the responsivity of the PQD-based phototransistors. The pure PBTTT transistor shows a mobility of 0.56 cm^2 V^{-1} s^{-1}, but in contrast, the field-effect mobility extracted from the saturated region (V_G = −40 V) shows that the PBT/PQD transistor has

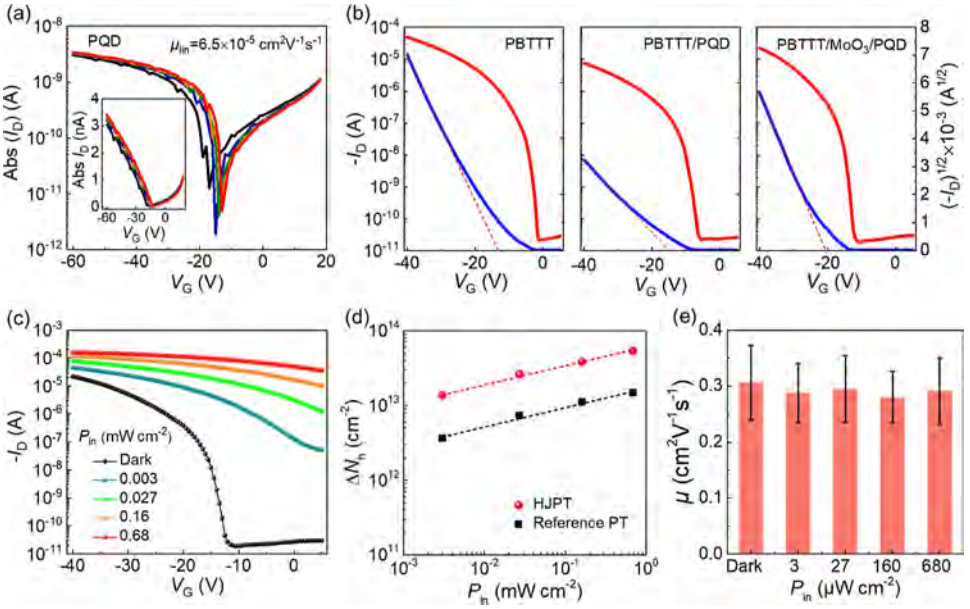

Figure 3. (a) Transfer characteristics of the pure PQD field-effect transistors in darkness with V_D fixed at −5 V (inset showing the corresponding linear changes); (b) transfer characteristics of the PBTTT, PBTTT/PQD, and the PBTTT/MoO_3/PQD field-effect transistors; (c) transfer characteristics of the HJPT for different illumination intensities when V_D is fixed at −40 V; (d) enhanced hole concentrations (ΔN_h) of the HJPTs and reference phototransistors for different P_{in}; (e) mobilities of the HJPTs in darkness and under light illumination for different P_{in}.

https://doi.org/10.1021/acsphotonics.2c01983
ACS Photonics 2023, 10, 764−771

a severely decreased average mobility of 0.18 $cm^2\ V^{-1}\ s^{-1}$. The lower carrier mobility can be attributed to the high-density defect states at the PBTTT/PQD interfaces created in the solution coating process, and a similar phenomenon has been observed by others. To solve this problem, an ultrathin MoO_3 interlayer is inserted between the PBTTT and PQD layers to improve the average carrier mobility to 0.36 $cm^2\ V^{-1}\ s^{-1}$, as compared to the device without the MoO_3 interlayer. The mobility enhancement stems from the MoO_3 interlayer, which reduces the defect states at the PBTTT/PQD interfaces and prevents PBTTT from degrading by the solvent during the subsequent solution processes. Although the carrier mobility is lower than that of the PBTTT transistors, it is still thousands of times higher than that of the PQD transistors, suggesting that the conduction channel is located at the PBTTT layer, and the current across the PQD layer is negligible due to the small carrier mobility. To evaluate the effects of the mobility on the photodetection characteristics, the carrier transit time (τ_{tran}) is calculated by the following equation: $\tau_{tran} = L^2/(\mu V_D)$, where L is the channel length, and μ is the hole mobility. For our devices with L of 40 μm, τ_{tran} is calculated to be on the order of 10 ms and 1 μs for the PQD and PBTTT/MoO_3/PQD transistors, respectively. The short τ_{tran} is critical to the high photogain and fast photoresponse because more holes can drift across the conduction channel during carrier recombination to increase the photocurrent.

The transfer characteristics of the HJPTs in darkness and under light irradiation (λ_{peak} = 513 nm) with different incident light intensities (P_{in}) are presented in Figure 3c. A reference phototransistor without PLA is fabricated for comparison, and the photodetection performance is shown in Figure S1 (Supporting Information). Here, V_G is swept from 5 to −40 V and V_D is fixed at −40 V. Upon light illumination, both the reference phototransistor and HJPT show a significant increment of the drain current I_D with higher P_{in}, indicating that P_{in} can modulate the charge carriers in the photoactive layer. Particularly, the increment in I_D of the HJPT is much bigger than that of the reference phototransistor for the same P_{in}. Given that both devices have the same device configuration except for the PLA coating, the higher photocurrent observed from the HJPT is mainly attributed to the polar polymer PLA. The large amount of strong electron-withdrawing moieties can trap separated electrons due to the CTE at the PQD/PLA interface, which further decreases the exciton recombination probability. Consequently, the CTE increases the hole concentration in the conduction channel and the photocurrent. Furthermore, the positive shift in the threshold voltage (ΔV_T) observed from both HJPT and reference phototransistors is caused by the photogating effect arising from the trapped photogenerated electrons and high-density holes in the conduction channel. The threshold voltage shifts of HJPT and reference PT under different light intensities are shown in Figure S2 (Supporting Information). In the reference phototransistors, electrons are more likely to recombine with photoholes, but in the HJPT, photoelectrons are effectively trapped at the PQD/PLA interface, thus producing a larger ΔV_T. For comparison, we estimate the enhanced hole concentration (ΔN_h) in both the HJPTs and reference phototransistors for different P_{in} according to the equation: $\Delta N_h = (C_i \times \Delta V_T)/e$, where C_i is the capacitance per unit area of the dielectric layer and e is the elementary charge. As shown in Figure 3d, ΔN_h is proportional to P_{in} regardless of the device type, and ΔN_h of the HJPT is larger than that of the reference phototransistors for the same P_{in}, further verifying efficient hole−electron pair separation in the HJPT due to the PLA. Figure 3e exhibits the mobilities of the HJPT device in darkness and under light illumination for different P_{in}. The mobilities are comparable whether the device is under light illumination or in the dark state, denoting that the mobility is not affected when the devices are operated in light.

The photodetection properties of the HJPT are evaluated systematically. Figure 4a shows the photosensitivity (I_{photo}/I_{dark}) of the HJPT as a function of V_G for different light intensities. The photosensitivity in the off-state with low dark currents ($V_G < -10$ V) is much higher than that in the on-state ($V_G > -10$ V) and the maximum photosensitivity is observed at the turn-on gate voltage ($V_G = -10$ V) because of the dual modulation of the charge carriers by both the incident light and gate voltage. The photosensitivity increases with incident light power and reaches a maximum of 8×10^6 at 0.68 mW cm^{-2}, which is almost two orders of magnitude higher than that of the reference device (Figure S1b, Supporting Information) under the same conditions. To further investigate the effects of the gate voltage and incident light on the photodetection properties, the responsivity (R) as a function of V_G for different light intensities is presented in Figure 4b, where R indicates how efficiently a photodetector responds to light and is given by the equation $R = I_{ph}/(P_{in}A)$, where I_{ph} is the photocurrent, P_{in} the incident light intensity, and A the photosensitive area (channel region) of the HJPT device. The maximum R is found to be 2.1×10^4 A W^{-1} for the smallest illumination power density of 3 $\mu W/cm^2$ at $V_G = -40$ V. The responsivity of our HJPT is among the best reported to date for PQD-based photodetectors.

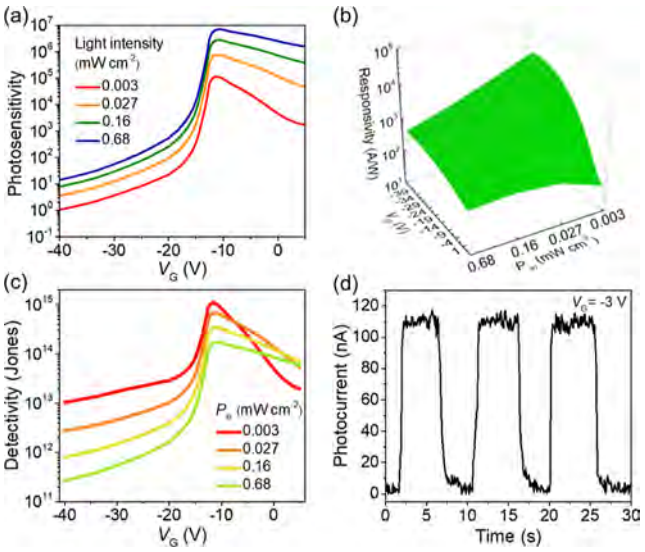

Figure 4. (a) Gate-voltage-dependent photosensitivity (P) of the HJPT under different light illumination; (b) photoresponsivity (R) and (c) specific detectivity (D^*) of the HJPT under irradiation at different gate voltages; (d) photocurrent switching behavior of the HJPT under alternating dark condition and light illumination.

It should be noted that the ultrahigh responsivity is achieved by sacrificing the dark current, and this should be considered in practice. Therefore, the responsivity in the low dark current region (off-state and subthreshold region) is evaluated. In the HJPT, an R value of 118 A W^{-1} is obtained at a gate bias of 0 V and a low dark current of 20 pA, and it is two orders of

https://doi.org/10.1021/acsphotonics.2c01983
ACS Photonics 2023, 10, 764−771

magnitude higher than that of the commercial silicon-based photodetectors (~1 A W^{-1}). The high responsivity, low operation voltage, and low dark current confirm the great practical potential. The specific detectivity (D^*) is another important figure-of-merit for photodetectors. It indicates the photosensitivity and the shot noise limit of photodetectors. Assuming that the dark current is dominated by the shot noise, D^* can be described as $D^* = RS^{1/2}(2eI_{dark})^{-1/2}$. Figure 4c presents the D^* values as a function of V_G for different light intensities at a fixed V_D of −40 V, where D^* shows a similar trend with I_{photo}/I_{dark} and reaches the peak at the turn-on gate voltage (i.e., −12 V). The peak of D^* of the HJPT is above 10^{14} Jones, and the maximum D^* is ~1 × 10^{15} Jones. The time-dependent photoresponse of the HJPT is assessed by measuring the change in I_D during on-and-off light illumination. As shown in Figure 4d, the HJPT exhibits a reproducible photodetection behavior under alternating dark conditions and light illumination, and the rise and decay times of the HJPT device are 0.4 and 0.8 s, respectively.

The ability to detect weak light is very important for photodetectors. Since the fluctuation of the dark current is the main factor that influences the detection of weak light signals, reducing the dark current is vital to phototransistors and realizing high signal-to-noise ratios (SNRs) and high detectivity. In our HJPT device, the conduction channel can be modulated by the gate voltage and completely turned off in the dark by operating the device in the depletion regime. The dark current of the HJPT is as low as ~20 pA at lateral biases of −10 and 0 V (Figure S3, Supporting Information), which is advantageous when detecting very weak signals. Figure 5a,b show the noise power spectra of the HJPT in the frequency range of 1 Hz−100 kHz with channel currents varying from 20 pA to 22 μA. The noise current is down to 1 × 10^{-14} A $Hz^{-1/2}$ at low frequencies when the device is operated in the off state (V_G = 0 and 5 V). The noise spectra follow the 1/f relationship in the frequency range from 1 Hz to 100 kHz at all gate voltages. However, the noise spectra of the HJPT in the off-states at higher frequencies (>10 kHz) are almost flat and independent of frequencies. The flat noise spectra indicate that noise in this area is dominated by thermal noise originating from the thermal random motion of charge carriers. Although charge carriers flow through the conduction channel as a whole, each charge carrier shows some random motion in various directions due to the limited gate effect at a low gate bias. Clearly, the ideal closed conduction channel in the off-state results in a small dark current and a small shot noise. When the device is turned on (V_G > −10 V), the noise current increases rapidly with the gate voltage and dark current. Besides the dark current shot noise, the optical shot noise due to the fluctuation of the photocurrent under light illumination affects weak signal detection. Therefore, we investigate the optical noise current by calculating the standard deviation of the photocurrents (Figure 5c), and a high SNR of 35.3 is obtained for a weak incident light of 3 μW/cm^2, meaning that the HJPT is capable of detecting much weaker light signals. The photoconductive gain is plotted as a function of dark currents for different incident light intensities in Figure 5d, where the dark current is measured at different gate voltages for a fixed V_D of −40 V. The HJPT exhibits high photoconductive gain, exceeding 10^3 for various incident light intensities and dark currents. A photoconductive gain plateau appears in the subthreshold region, implying that the photoconductive gain can be maintained even when the dark current density decreases as the transistor enters the off state.

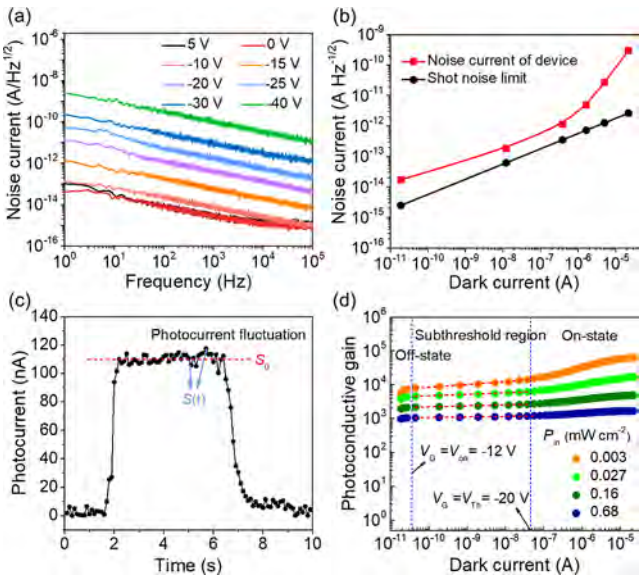

Figure 5. (a) Noise current spectra of the HJPT in different channel current states (dark current); (b) noise current at 100 Hz against dark currents and the shot noise given by $I_{shot} = Sqrt\ (2qI_{dark})$; (c) optical shot noise due to the photocurrent fluctuation; (d) photoconductive gain as a function of dark currents for various incident light intensities.

The long-term stability and light exposure lifetime are key challenges for practical applications of organic and perovskite-based photodetectors. Both organic semiconductors and perovskites normally suffer from severe oxygen/moisture degradation under ambient conditions, leading to deterioration or even failure. Device degradation can also be caused by photo-oxidation, which should be taken into account when the devices are used in the presence of light. As the PQD/OSC heterojunction is covered by a polar polymer, PLA, besides the charge trapping effect, the PLA layer also serves as an encapsulation layer to protect the device from oxygen/moisture degradation. Therefore, the long-term stability of the PLA/PQD/PBTTT phototransistors is assessed in ambient conditions. As shown in Figure 6a, the transfer curves in the dark and under light illumination are recorded randomly for 120 days, and the PLA coating provides pronounced protection, as shown by the stable and reproducible output current throughout the period. The photoresponsivity and dark/photo current as functions of time are shown in Figures 6b and S4 (Supporting Information), respectively. 95% retention of the photoresponsivity is accomplished after storing for 120 days, but for the reference PTs without PLA, the photoresponsivity drops to 62% under the same conditions. Obviously, the phototransistors are more stable due to the excellent oxygen/moisture resistance provided by the PLA coating. In fact, if we define the phototransistor lifetime as the time it takes to degrade to 60% of the initial photoresponsivity, the lifetime is estimated to be 23,000 h by extending the linear degradation plot. To examine the stability of the HJPT under continuous and strong light illumination, continuous light exposure is conducted under the same ambient conditions as aforementionaed (Figure 6c). The phototransistor is irradiated continuously with strong while light with an intensity of 10 mW/cm^2 under ambient conditions. When the transfer curves are acquired under

https://doi.org/10.1021/acsphotonics.2c01983
ACS Photonics 2023, 10, 764−771

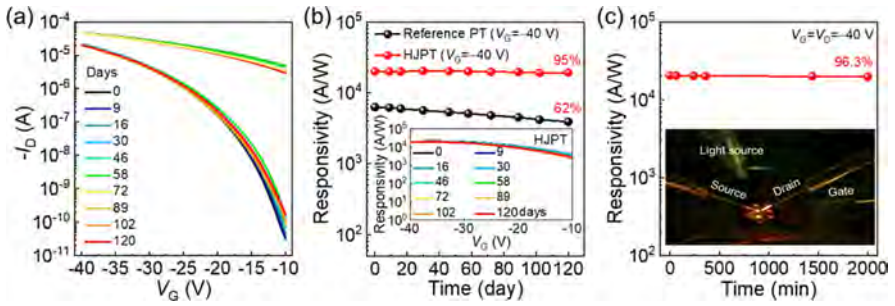

Figure 6. (a) Transfer curves in ambient air with 40−50% humidity in darkness and under 10 μW/cm^2 at V_D = −40 V; (b) drain current output in darkness and under 10 μW/cm^2; (c) photoresponsivity in ambient air under continuous strong white light illumination (10 mW/cm^2). Inset: photograph showing continuous light exposure.

illumination, the light source is turned off for 10 min, and then 513 nm monochromatic light with an intensity of 3 μW/cm^2 is turned on. As shown in Figure 6c, 96% of the initial photoresponsivity is maintained after 2000 min of continuous light illumination, which again indicates the superior stability of the HJPT. The light exposure lifetime is estimated to be 21,600 min based on the same approach. Since the light intensity is usually lower than 1 mW/cm^2 in the majority of phototransistor applications, the light exposure lifetime will be much longer than that estimated in our experiments. Besides the role as a physical barrier, PLA offers fast electron transfer due to the charge-trapping effect and reduces the photo-oxidation probability to a certain extent, partly because the photo-oxidation rate depends on the relative rates of oxidation and electron transfer.

3. CONCLUSIONS

A novel device concept based on the polar polymer-capped perovskite quantum dots/organic semiconductor heterojunction is demonstrated for organic phototransistors. This device architecture takes advantage of high light absorption, a charge trapping effect, and efficient carrier transport to achieve high-gain and ultrasensitive photodetection. The fabricated HJPTs deliver outstanding photodetection performance, such as a high photosensitivity of 1.5×10^4, a photoresponsivity of 2.1×10^4 A/W, a photodetectivity of 1×10^{15} Jones, and a high gain of 6.4×10^4, when exposed to weak incident light with a power of 3 μW/cm^2. The polar polymer capping layer improves the device stability. The mechanism and strategy demonstrated in this work can be extended to other systems and are applicable to photodetection spanning the UV and NIR regimes. The device structure and concept have broad and promising application potential pertaining to high-performance organic optoelectronics.

4. EXPERIMENTAL SECTION

4.1. Materials and Device Fabrication. PBTTT was purchased from Luminescence Technology Corp. (Lumtec) and used without further purification, and $CsPbBrI_2$ QDs were bought from MKNANO. The phototransistors were fabricated with the bottom-gate/bottom-contact configuration on the SiO_2/p$^+$-Si(100) substrate. p$^+$-Si and thermally grown SiO_2 (250 nm) served as the gate and dielectric layers, respectively. The SiO_2/Si substrate was sequentially ultrasonicated in acetone, isopropanol, and deionized water for 10 min each and then treated with UV/ozone for 15 min. The SiO_2/Si substrate was immersed in 0.1 mol/L octyltrichlorosilane (OTS) in anhydrous toluene for 30 min at 60 °C. The surface-modified substrate was rinsed with anhydrous toluene and ultrasonicated in fresh anhydrous toluene to remove the excess multilayer OTS and dried under flowing N_2. The PBTTT-C14 solution was prepared by dissolving PBTTT-C14 in 1,2-dichlorobenzene (*o*-DCB) and stirring for 12 h at 60 °C.

The Ti/Au source and drain electrodes (5 nm/60 nm) were evaporated thermally on the pretreated substrate through a shadow mask. The channel length (L) of the OPT devices was varied from 40 μm to 100 μm with a fixed W/L of 10. The organic semiconductor channel layer was first deposited by spin coating using ∼0.5 wt % solutions in warm *o*-DCB at 3000 rpm for 40 s. The as-coated films were then heated to 180 °C on a hot plate, followed by a slow cooling to room temperature. After organic semiconductor deposition, the PQD light-absorbing layer was deposited by spin coating at 1000 rpm for 40 s. The samples were then put under vacuum for 1 h to remove the solvent. Finally, the PLA layers were deposited by spin coating with the 10 mg/mL solution in chloroform at 3000 rpm for 40 s and then heated to 60 °C for 1 h under vacuum to remove the residual solvent. The entire transistor fabrication process was carried out in a nitrogen-filled glove box. All the solutions (except the PQD solution) were filtered with an acrodisc PTFE syringe filter (Millipore 0.45 μm) prior to spin coating. For the reference PTs, the samples underwent the same cleaning, film-deposition, and metal-evaporation processes, except spin-coating of the PLA layer.

4.2. Electrical and Optoelectronic Characterization. Electrical characterization of the phototransistors was carried out in air on the Primarius FS-Pro semiconductor parameter analyzer with a standard probe station. Optoelectronic characterization was performed by determining the transfer characteristics of the devices in darkness and under various light illumination intensities using a tungsten lamp/monochrometer system with tunable wavelengths (200−1200 nm) and intensity. During light detection, the phototransistors and light source were placed in a metal box to avoid the influence of ambient light. The intensity of the incident light at different wavelengths was calibrated by a commercial silicon photodetector.

4.3. Characterization of the Organic Films. The ultraviolet−visible (UV−vis) transmission measurements were performed on the JASCO V-570 spectrophotometer. The samples were prepared on quartz substrates using the same deposition parameters described above. Atomic force microscopy was carried out in the tapping mode on the MultiMode 8 (Bruker) atomic force microscope in a glove box.

https://doi.org/10.1021/acsphotonics.2c01983
ACS Photonics 2023, 10, 764−771

4.4. Photoluminescence and Lifetime Measurements. The steady-state and transient photoluminescence (PL) spectra were recorded at an excitation wavelength of 510 nm and slit widths of 5 mm on a commercial spectrofluorometer (Horiba, Fluorolog). A 400 nm laser was used as an excitation source, which was generated by the second harmonic of the lithium niobate crystal using a picosecond laser (EKSPLA, PLD240) with a tunable wavelength set at 800 nm, pulse duration of 3 ps, and repetition rate of 86 MHz. The laser beam was focused onto the sample to a spot diameter of about 500 nm through a 100× microscope objective with N.A. = 0.75. The reflected light and fluorescence were collimated by the same objective and reflected by a beam splitter before importing into a spectrometer (HORIBA, iHR550). A 425 nm long-pass filter was utilized to filter the scattered laser background signal. The fluorescence signal was coupled into the spectrometer in free space or by a fiber controlled by a flip silver mirror. The fiber collecting port was coupled to a single photon detector (MPD, PD-100-CTD-FC, time resolution ≈ 30 ps) in the time delay measurement by the time-correlated single photon counting method.

■ ASSOCIATED CONTENT

Supporting Information

The Supporting Information is available free of charge at https://pubs.acs.org/doi/10.1021/acsphotonics.2c01983.

Photodetection performance of the reference OPT; threshold voltage shift of HJPT and reference PT; dark current stability of the HJPT; and dark current and photocurrent of the HJPT as a function of time (PDF)

■ AUTHOR INFORMATION

Corresponding Author

Jia Li − *College of Engineering Physics, Shenzhen Technology University, Shenzhen 518118, P. R. China; Key Laboratory of Aerospace Information Materials and Physics, MIIT, Nanjing University of Aeronautics and Astronautics, Nanjing 211106, P. R. China;* orcid.org/0000-0002-2270-9876; Email: lijia@sztu.edu.cn

Authors

Yuanhong Gao − *School of Advanced Materials, Shenzhen Graduate School, Peking University, Shenzhen 518055, P. R. China*

Shuai Sun − *College of Engineering Physics, Shenzhen Technology University, Shenzhen 518118, P. R. China*

Dan Qiu − *College of Engineering Physics, Shenzhen Technology University, Shenzhen 518118, P. R. China*

Yu-Ming Wei − *State Key Laboratory of Optoelectronic Materials and Technologies, School of Physics, Sun Yat-sen University, Guangzhou 510275, P. R. China*

Mengpei Zhang − *College of Engineering Physics, Shenzhen Technology University, Shenzhen 518118, P. R. China*

Jin Liu − *State Key Laboratory of Optoelectronic Materials and Technologies, School of Physics, Sun Yat-sen University, Guangzhou 510275, P. R. China;* orcid.org/0000-0001-5727-6874

Paul K. Chu − *Department of Physics, Department of Materials Science and Engineering, and Department of Biomedical Engineering, City University of Hong Kong, Kowloon, Hong Kong, P. R. China;* orcid.org/0000-0002-5581-4883

Wen-Long You − *Key Laboratory of Aerospace Information Materials and Physics, MIIT, Nanjing University of Aeronautics and Astronautics, Nanjing 211106, P. R. China*

Complete contact information is available at: https://pubs.acs.org/10.1021/acsphotonics.2c01983

Funding

This work was supported by the National Natural Science Foundation of China (11974371); the Science and Technology Planning Project of the Guangdong Province of China (2021A0505110012); Shenzhen Science and Technology Research Funding (JCYJ20180507182429941); Scientific Research Start-Up Fund of SZTU (GDRC202140); Opening Fund of the Key Laboratory of Aerospace Information Materials and Physics (Nanjing University of Aeronautics and Astronautics), MIIT; City University of Hong Kong Donation Research Grant (DON-RMG 9229021); and Shenzhen—Hong Kong Innovative Collaborative Research and Development Program (SGLH20181109110802117 and CityU 9240014).

Notes

The authors declare no competing financial interest.

■ REFERENCES

(1) Pierre, A.; Gaikwad, A.; Arias, A. C. Charge-Integrating Organic Heterojunction Phototransistors for Wide-Dynamic-Range Image Sensors. *Nat. Photonics* **2017**, *11*, 193−199.

(2) Chow, P. C. Y.; Matsuhisa, N.; Zalar, P.; Koizumi, M.; Yokota, T.; Someya, T. Dual-Gate Organic Phototransistor with High-Gain and Linear Photoresponse. *Nat. Commun.* **2018**, *9*, 4546.

(3) Calvi, S.; Rapisarda, M.; Valletta, A.; Scagliotti, M.; De Rosa, S.; Tortora, L.; Branchini, P.; Mariucci, L. Highly Sensitive Organic Phototransistor for Flexible Optical Detector Arrays. *Org. Electron.* **2022**, *102*, 106452.

(4) Huang, X.; Li, Q.; Shi, W.; Liu, K.; Zhang, Y.; Liu, Y.; Wei, X.; Zhao, Z.; Guo, Y.; Liu, Y. Dual-Mode Learning of Ambipolar Synaptic Phototransistor Based on 2D Perovskite/Organic Heterojunction for Flexible Color Recognizable Visual System. *Small* **2021**, *17*, 2102820.

(5) Lochner, C. M.; Khan, Y.; Pierre, A.; Arias, A. C. All-Organic Optoelectronic Sensor for Pulse Oximetry. *Nat. Commun.* **2014**, *5*, 5745.

(6) Chen, M.; Lu, H.; Abdelazim, N. M.; Zhu, Y.; Wang, Z.; Ren, W.; Kershaw, S. V.; Rogach, A. L.; Zhao, N. Mercury Telluride Quantum Dot Based Phototransistor Enabling High-Sensitivity Room-Temperature Photodetection at 2000 nm. *ACS Nano* **2017**, *11*, 5614−5622.

(7) Xu, H.; Liu, J.; Zhang, J.; Zhou, G.; Luo, N.; Zhao, N. Flexible Organic/Inorganic Hybrid Near-Infrared Photoplethysmogram Sensor for Cardiovascular Monitoring. *Adv. Mater.* **2017**, *29*, 1700975.

(8) Song, J.; Lin, P.; Ruan, Y. F.; Zhao, W. W.; Wei, W.; Hu, J.; Ke, S.; Zeng, X.; Xu, J. J.; Chen, H. Y.; Ren, W.; Yan, F. Organic Photo-Electrochemical Transistor-Based Biosensor: A Proof-of-Concept Study toward Highly Sensitive DNA Detection. *Adv. Healthcare Mater.* **2018**, *7*, 1800536.

(9) Yang, J.; Li, G.; Wang, W.; Shi, J.; Li, M.; Xi, N.; Zhang, M.; Liu, L. A Bio-Syncretic Phototransistor Based on Optogenetically Engineered Living Cells. *Biosens. Bioelectron.* **2021**, *178*, 113050.

(10) Cao, Y.; Ge, Y.; Sha, X.; Meng, L.; Gao, Y.; Li, B.; Yu, X.-F.; Li, J. Sensitive Direct X-Ray Detectors Based on the In−Ga−Zn−O/Perovskite Heterojunction Phototransistor. *Flexible Printed Electron.* **2022**, *7*, 014013.

(11) Gao, Y.; Ge, Y.; Wang, X.; Liu, J.; Liu, W.; Cao, Y.; Gu, K.; Guo, Z.; Wei, Y. M.; Zhou, N.; Yu, D.; Meng, H.; Yu, X. F.; Zheng, H.; Huang, W.; Li, J. Ultrathin and Ultrasensitive Direct X-ray Detector Based on Heterojunction Phototransistors. *Adv. Mater.* **2021**, *33*, 2101717.

(12) Gansen, E. J.; Rowe, M. A.; Greene, M. B.; Rosenberg, D.; Harvey, T. E.; Su, M. Y.; Hadfield, R. H.; Nam, S. W.; Mirin, R. P. Photon-Number-Discriminating Detection Using a Quantum-Dot, Optically Gated, Field-Effect Transistor. *Nat. Photonics* **2007**, *1*, 585−588.
(13) Hadfield, R. H. Single-Photon Detectors for Optical Quantum Information Applications. *Nat. Photonics* **2009**, *3*, 696−705.
(14) Zhou, Y.; Wang, Y. *Perovskite Quantum Dots Synthesis, Properties and Applications*; Springer Singapore, Imprint, Springer, 2020; p 9789811566370.
(15) Chen, Y.; Chu, Y.; Wu, X.; Ou-Yang, W.; Huang, J. High-Performance Inorganic Perovskite Quantum Dot-Organic Semiconductor Hybrid Phototransistors. *Adv. Mater.* **2017**, *29*, 1704062.
(16) Liu, K.; Bian, Y.; Kuang, J.; Huang, X.; Li, Y.; Shi, W.; Zhu, Z.; Liu, G.; Qin, M.; Zhao, Z.; Li, X.; Guo, Y.; Liu, Y. Ultrahigh-Performance Optoelectronic Skin Based on Intrinsically Stretchable Perovskite-Polymer Heterojunction Transistors. *Adv. Mater.* **2022**, *34*, 2107304.
(17) Chen, K.; Zhang, X.; Chen, P. A.; Guo, J.; He, M.; Chen, Y.; Qiu, X.; Liu, Y.; Chen, H.; Zeng, Z.; Wang, X.; Yuan, J.; Ma, W.; Liao, L.; Nguyen, T. Q.; Hu, Y. Solution-Processed CsPbBr(3) Quantum Dots/Organic Semiconductor Planar Heterojunctions for High-Performance Photodetectors. *Adv. Sci.* **2022**, *9*, 2105856.
(18) Pradhan, B.; Das, S.; Li, J.; Chowdhury, F.; Cherusseri, J.; Pandey, D.; Dev, D.; Krishnaprasad, A.; Barrios, E.; Towers, A.; Gesquiere, A.; Tetard, L.; Roy, T.; Thomas, J. Ultrasensitive and Ultrathin Phototransistors and Photonic Synapses Using Perovskite Quantum Dots Grown from Graphene Lattice. *Sci. Adv.* **2020**, *6*, No. eaay5225.
(19) Cao, Y.; Sha, X.; Bai, X.; Shao, Y.; Gao, Y.; Wei, Y. M.; Meng, L.; Zhou, N.; Liu, J.; Li, B.; Yu, X. F.; Li, J. Ultralow Light-Power Consuming Photonic Synapses Based on Ultrasensitive Perovskite/Indium-Gallium-Zinc-Oxide Heterojunction Phototransistors. *Adv. Electron. Mater.* **2021**, *8*, 2100902.
(20) Zou, C.; Xi, Y. Y.; Huang, C. Y.; Keeler, E. G.; Feng, T. Y.; Zhu, S. H.; Pozzo, L. D.; Lin, L. Y. A Highly Sensitive UV-vis-NIR All-Inorganic Perovskite Quantum Dot Phototransistor Based on a Layered Heterojunction. *Adv. Opt. Mater.* **2018**, *6*, 1800324.
(21) Xie, C.; You, P.; Liu, Z.; Li, L.; Yan, F. Ultrasensitive Broadband Phototransistors Based on Perovskite/Organic-Semiconductor Vertical Heterojunctions. *Light Sci. Appl.* **2017**, *6*, No. e17023.
(22) Lv, W.; Li, L.; Xu, M.; Hong, J.; Tang, X.; Xu, L.; Wu, Y.; Zhu, R.; Chen, R.; Huang, W. Improving the Stability of Metal Halide Perovskite Quantum Dots by Encapsulation. *Adv. Mater.* **2019**, *31*, 1900682.
(23) Kwak, D. H.; Lim, D. H.; Ra, H. S.; Ramasamy, P.; Lee, J. S. High Performance Hybrid Graphene-CsPbBr3-XIx Perovskite Nanocrystal Photodetector. *RSC Adv.* **2016**, *6*, 65252−65256.
(24) Huang, J.; Du, J.; Cevher, Z.; Ren, Y. H.; Wu, X. H.; Chu, Y. L. Printable and Flexible Phototransistors Based on Blend of Organic Semiconductor and Biopolymer. *Adv. Funct. Mater.* **2017**, *27*, 1604163.
(25) Xu, H.; Li, J.; Leung, B. H.; Poon, C. C.; Ong, B. S.; Zhang, Y.; Zhao, N. A High-Sensitivity Near-Infrared Phototransistor Based on an Organic Bulk Heterojunction. *Nanoscale* **2013**, *5*, 11850−11855.
(26) Zhang, Y.; Yuan, Y.; Huang, J. Detecting 100 fW cm(-2) Light with Trapped Electron Gated Organic Phototransistors. *Adv. Mater.* **2017**, *29*, 1603969.
(27) Gao, Y.; Yi, Y.; Wang, X.; Meng, H.; Lei, D.; Yu, X. F.; Chu, P. K.; Li, J. A Novel Hybrid-Layered Organic Phototransistor Enables Efficient Intermolecular Charge Transfer and Carrier Transport for Ultrasensitive Photodetection. *Adv. Mater.* **2019**, *31*, 1900763.
(28) Chu, Y.; Wu, X.; Lu, J.; Liu, D.; Du, J.; Zhang, G.; Huang, J. Photosensitive and Flexible Organic Field-Effect Transistors Based on Interface Trapping Effect and Their Application in 2D Imaging Array. *Adv. Sci.* **2016**, *3*, 1500435.
(29) Jones, D.; An, Y.; Hidalgo, J.; Evans, C.; Vagott, J. N.; Correa-Baena, J. P. Polymers and Interfacial Modifiers for Durable Perovskite Solar Cells: a review. *J. Mater. Chem. C* **2021**, *9*, 12509−12522.
(30) Hintermayr, V. A.; Lampe, C.; Löw, M.; Roemer, J.; Vanderlinden, W.; Gramlich, M.; Böhm, A. X.; Sattler, C.; Nickel, B.; Lohmüller, T.; Urban, A. S. Polymer Nanoreactors Shield Perovskite Nanocrystals from Degradation. *Nano Lett.* **2019**, *19*, 4928−4933.

https://doi.org/10.1021/acsphotonics.2c01983
ACS Photonics 2023, 10, 764−771

Supporting Information

Hybrid Interfacial Engineering: An Enabling Strategy for Highly Sensitive and Stable Perovskite Quantum Dots / Organic Heterojunction Phototransistors

*Yuanhong Gao,[1] Shuai Sun,[2] Dan Qiu,[2] Yu-Ming Wei[3], Mengpei Zhang,[2] Jin Liu,[3] Paul K. Chu,[4] Wen-Long You,[5] and Jia Li [2,5]**

[1]School of Advanced Materials, Shenzhen Graduate School, Peking University, Shenzhen 518055, P. R. China

[2] College of Engineering Physics, Shenzhen Technology University, Shenzhen 518118, P. R. China

[3] State Key Laboratory of Optoelectronic Materials and Technologies, School of Physics, Sun Yat-sen University, Guangzhou 510275, P. R. China

[4] Department of Physics, Department of Materials Science and Engineering, and Department of Biomedical Engineering, City University of Hong Kong, Tat Chee Avenue, Kowloon, Hong Kong, P. R. China

[5] Key Laboratory of Aerospace Information Materials and Physics，(Nanjing University of Aeronautics and Astronautics), MIIT, Nanjing 211106, P. R. China

AUTHOR INFORMATION

Corresponding Author

*Email: lijia@sztu.edu.cn (J. Li)

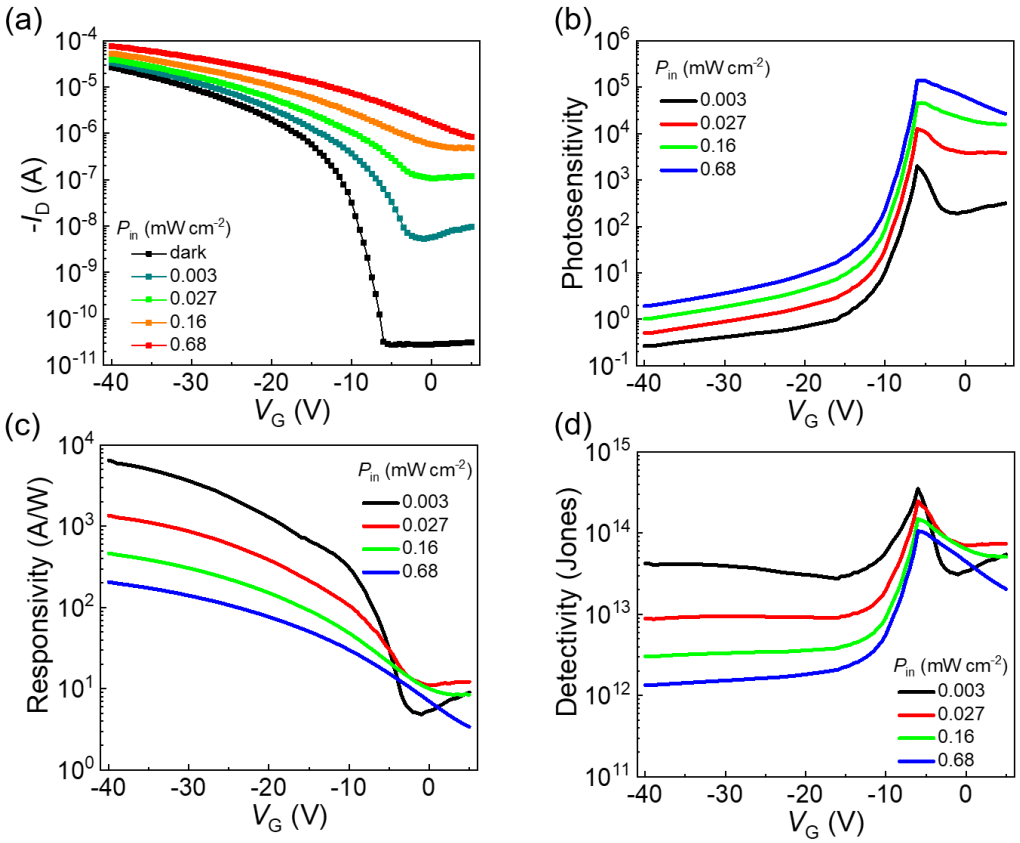

Figure S1. Photodetection performance of the reference OPT. (a) Transfer characteristics of HJPT under different illumination intensities when V_D is fixed at −40 V. (b) Gate-voltage dependent photosensitivity (P) of the reference PT under different light illumination. Photoresponsivity (R), and (c) Specific Detectivity (D*) of the reference PT under irradiation at different gate voltages.

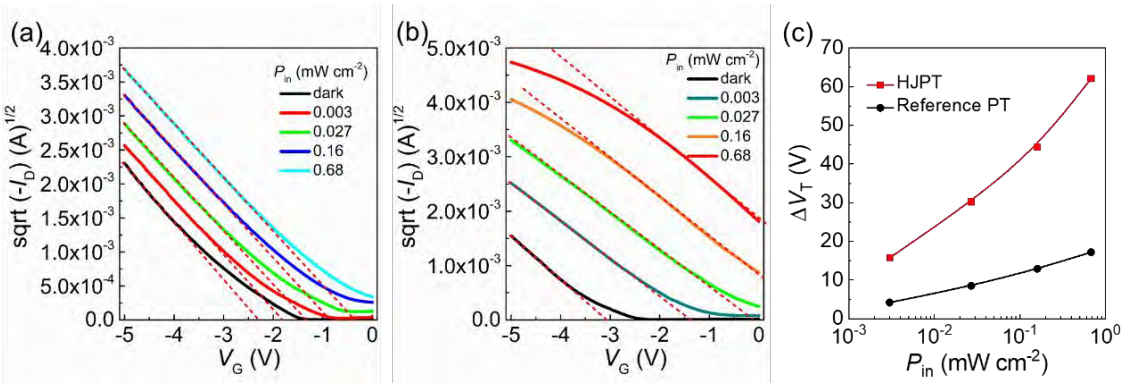

Figure S2. Threshold voltage shift of (a) HJPT and (b) reference OPT under different light intensities. (c) Threshold voltage shift as a function of incident light intensity.

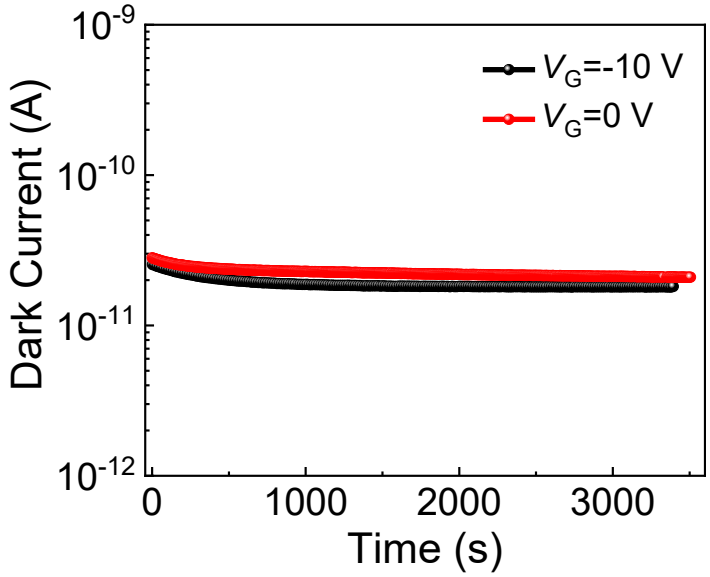

Figure S3. Dark current stability of the HJPT under different gate voltage bias and the same V_D of -40 V.

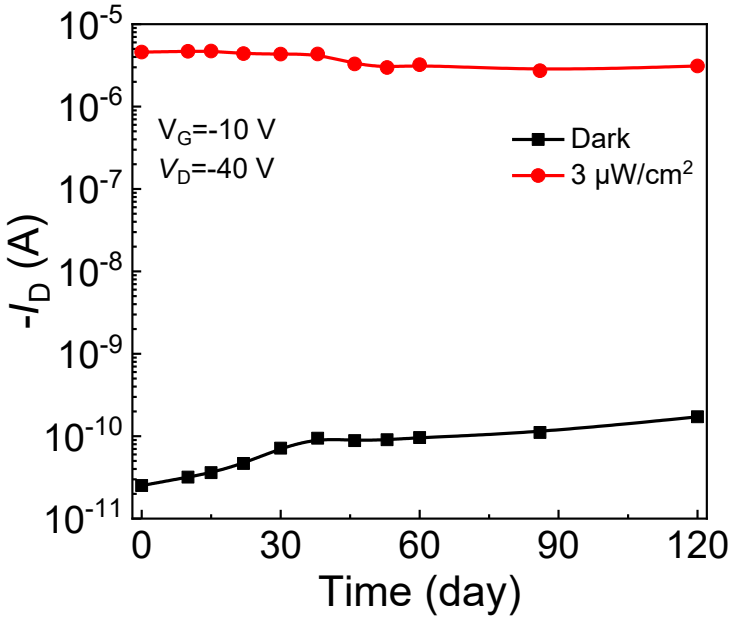

Figure S4. Dark current and photocurrent of the HJPT as a function of time.